




Cite this: *Dalton Trans.*, 2018, **47**, 357

Is a strong axial crystal-field the only essential condition for a large magnetic anisotropy barrier? The case of non-Kramers Ho(III) versus Tb(III) †

Sandeep K. Gupta,  Thayalan Rajeshkumar, Gopalan Rajaraman * and Ramaswamy Murugavel *

A monometallic non-Kramers Ho(III) complex with a strong uniaxial ligand field displays a record high energy barrier of 355 K with hysteresis opening up to 4 K at a sweep rate of 0.027 T s⁻¹, while the isomorphous, more anisotropic non-Kramers Tb(III) complex displays strong quantum tunnelling between the ground states. *Ab initio* calculations reveal that the presence of strong axial ligands and moderately weaker equatorial ligands is sufficient to quench the QTM between the ground pseudo doublets ($m_J = \pm 8$) in the case of Ho(III) complex, where the relaxation is found to proceed *via* the first excited state. However, the equatorial field disrupts the stabilization of ground pseudo doublets in Tb(III), inducing QTM and inhibiting SIM behaviour. Further insights into the decisive role played by the secondary coordination sphere and hydrogen-bonding in the SIM characteristics of these two non-Kramers ions were also gained. This combined experimental and computational approach highlights that although strong axiality holds the key for designing high temperature SIMs based on oblate non-Kramers ions, the strength of the equatorial ligand field also cannot be ignored.

Received 26th October 2017,
Accepted 24th November 2017
DOI: 10.1039/c7dt04020b

rsc.li/dalton

Introduction

Since 2003, investigations on single molecule magnets (SMMs) that are potential candidates for high-density storage and molecular spintronics based devices have seen a humongous shift from molecular systems that employ transition metal ions to heavier lanthanide ions that possess strong negative spin-orbit coupling.¹ In the case of lanthanide complexes, single-ion magnets (SIMs)/SMMs are, however, very disposed to fast quantum tunnelling of magnetisation (QTM). QTM can be quenched either by employing a strong magnetic exchange or by incorporating 3d ions into the cluster.² SIMs with high $\pm m_J$ ground-state magnetic doublets with significant separation from the excited $\pm m_J$ sub-levels have been obtained counting on the symmetry and the ligand field around the Ln(III) ions.³ However, much emphasis has revolved around Tb(III), Dy(III) and Er(III) complexes, leaving SMMs based on 4f ions such as Ho(III) relatively rare.^{4,2d,5} The ideal SIM for potential applications is predicted to be a low-coordinate complex,

especially in a linear two-coordinate geometry, resulting in relaxation *via* the highest excited state.⁶ However, the situation is more complicated due to the large ionic radii of 4f ions that tend to form complexes with higher coordination numbers. The combination of strong axial coordination and higher molecular symmetry has led to the observation of barrier heights as large as 1277 cm⁻¹ with blocking temperatures approaching 60 K.^{3i,7}

In SIMs, the role of symmetry and the crystal field (CF) are the two most prominent factors that have been found to influence the magnetic anisotropy barrier for slow relaxation and the blocking temperature. The role of CF could be categorized into two types. The first one is the direct impact of the CF exerted by the ligands around the electron density of metal ions, which has been well accounted by Long *et al.*^{3a} The other way is to place closed-shell diamagnetic metal ions that indirectly influence the CF around the first coordination sphere of the paramagnetic ions in SIMs.⁸ Starting from the first known 4f SIMs such as {TbPc₂} reported by Ishikawa *et al.*,⁹ SIMs derived from ligands and their derivatives such as cyclooctatetraene (COT)^{4d,10} and phthalocyanine^{9,11} with higher order symmetry have led to a momentous increase in the anisotropy barrier. During this course, recent interest in D_{5h} possessing Ln(III) complexes bloomed, resulting in some of the highest reported barrier heights and blocking temperatures for any discrete air-stable magnetically active complex.^{3b-i}

Department of Chemistry, Indian Institute of Technology Bombay, Mumbai-400076, India. E-mail: rajaraman@chem.iitb.ac.in, rmv@chem.iitb.ac.in

† Electronic supplementary information (ESI) available: Crystallographic details, magnetic studies and quantum mechanical calculations. CCDC 1451541 (1), 1451545 (2) and 1548008 (1'). For ESI and crystallographic data in CIF or other electronic format see DOI: 10.1039/c7dt04020b

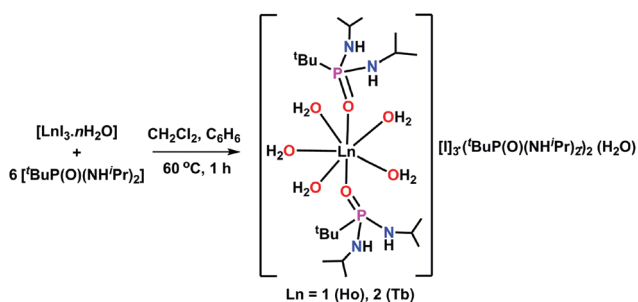
Thus it becomes necessary to evaluate whether this proxy approach of maintaining a strong axial CF works well with other 4f ions. This is particularly true as the nature of *prolativity/oblativity* is found to vary across various lanthanide ions.¹²

With this in mind, we have selected pseudo-linear complexes of Tb(III) (ground term symbol 7F_6) and Ho(III) (ground term symbol 5I_8), where both the ions naturally occur as only one stable isotope, for a comparative study. These two non-Kramers ions are recently gaining greater attention, being naturally present as one stable isotope, as suitable candidates for designing qubits that promise to reduce the decoherence due to hyperfine interactions. The recent observation of a long coherence time in pseudo-axial D_{4d} symmetric $[\text{Ho}(\text{W}_5\text{O}_{18})_2]^{9-}$ ions¹³ further underlines the importance of Ho(III) in SMMs. A Tb(III) complex with a more anisotropic oblate electronic charge distribution is expected to exhibit a higher anisotropy barrier than a Ho(III) complex. In contrast, we wish to show that a Ho(III) complex (**1**) with stronger axial ligation exhibits hysteresis up to 4 K, while the isomorphous Tb(III) complex (**2**) displays strong quantum tunnelling between the ground states leading to the absence of SIM behaviour in zero field. Detailed magnetic and theoretical studies based on the CASSCF/RASSI-SO/SINGLE_ANISO approach have been undertaken to probe the difference in the observed properties.

Results and discussion

Synthetic aspects

The organophosphonic diamide incorporating sterically bulky iso-propyl and *tert*-butyl groups, ${}^t\text{BuPO}(\text{NH}^i\text{Pr})_2$ (**L**),¹⁴ has been employed to stabilize lanthanide ions in the present study. The seven coordinate Ho(III) or Tb(III) organophosphonic diamide complexes were prepared from a direct reaction of the respective rare-earth triiodide hydrate and the phosphonic diamide in a 1 : 6 molar ratio in a dichloromethane–benzene solvent mixture (4 : 1, v/v) (Scheme 1). The reaction mixture was refluxed at 60 °C for 1 h and then allowed to slowly cool to room temperature. The clear filtrate was allowed to stand at room temperature for crystallisation. Single crystals of $[\text{L}_2\text{Ln}(\text{H}_2\text{O})_5][\text{I}_3] \cdot \text{L}_2 \cdot (\text{H}_2\text{O})$ [Ln = Ho (**1**); Tb (**2**); L = ${}^t\text{BuPO}(\text{NH}^i\text{Pr})_2$]



Scheme 1 Synthesis of the rare-earth seven-coordinate complexes **1** and **2**.

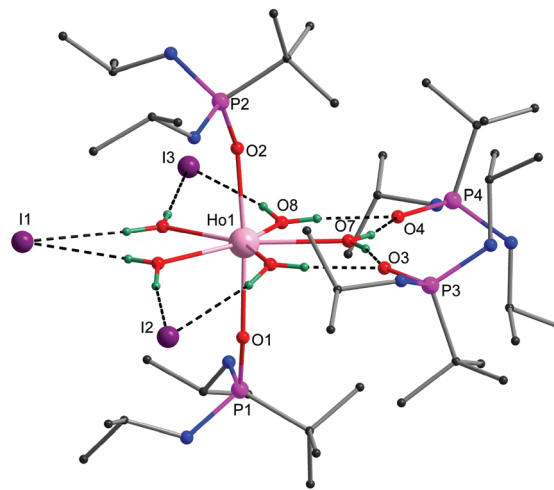


Fig. 1 (a) Molecular structure of **1**. Lattice water molecules and most of the H-atoms have been omitted for clarity. Dashed lines indicate hydrogen bonds.

were characterized by both analytical and spectroscopic techniques.

Molecular structures

Single crystal X-ray diffraction studies carried out on **1** and **2** revealed that they crystallize in the centrosymmetric triclinic space group $P\bar{1}$. The molecular structures of **1** (Fig. 1) and **2** share isostructural features with those of previously reported Dy(III) and Er(III) analogues.^{3b} The seven coordinate Ln(III) ions show minimal deviation from the ideal pentagonal bipyramidal geometry with a pseudo- D_{5h} environment around the central metal ion (Fig. 2 and Table S3†). Stronger ligation on the axial sites (average O–Ln distance = 2.194 Å (**1**) and 2.227 Å (**2**)) through the oxygen atoms of the neutral ligand **L** and considerably longer equatorial bonds (average O(aqua)–Ln distance = 2.343 Å (**1**) and 2.380 Å (**2**)) aided by near linear *trans*-O1–Ln–O2 angles provides an apparent pseudo-linear two coordinate environment to the central Ln(III) ions with strong axial fields. The nearest lattice metal–metal distances in **1** and **2** are 10.822 and 10.838 Å, respectively.

Magnetic studies

Direct current (dc) susceptibility measurements carried out on a polycrystalline sample of **1** under an applied field of 1000 Oe show a $\chi_M T$ value of 13.8 cm³ K mol^{−1} at 300 K that slowly decreases to 12.67 cm³ K mol^{−1} at 2 K (Fig. 3). A sharp decrease in $\chi_M T$ is, however, observed below 10 K, indicating the presence of magnetic blocking. However, no divergence was observed in the zero-field cooled and field-cooled magnetic susceptibility data. At 2 K, the magnetisation of **1** sharply rises to 4.89 μ_B at 2.0 T and remains almost constant before reaching 5.02 μ_B at 7.0 T (Fig. S2a†). The reduced magnetisation data are, however, superimposable on the isotherms (Fig. S3†). These observations on the temperature dependence of $\chi_M T$ and the field dependence of magnetisation indicate the

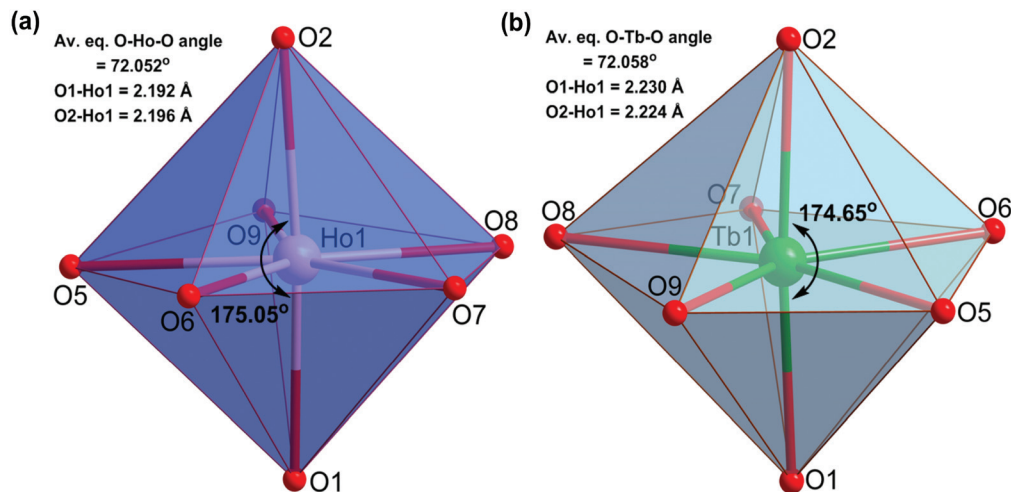


Fig. 2 Comparative polyhedral view of the pentagonal bipyramidal coordination environment of Ho(III) and Tb(III) with ligating oxygen atoms in **1** (a) and **2** (b), respectively.

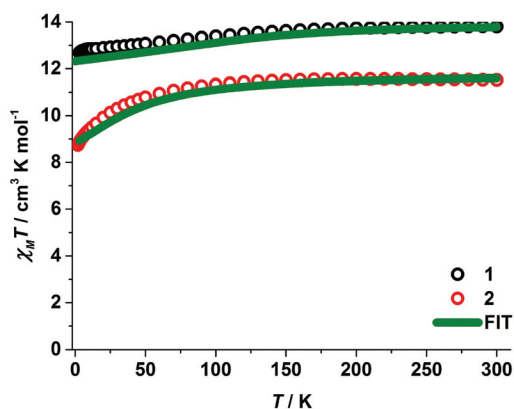


Fig. 3 Experimental and *ab initio* CASSCF computed temperature dependence of $\chi_M T$ product at 1000 Oe for **1** and **2**. Hollow circles correspond to the experimental magnetic susceptibility data and solid lines represent the computed magnetic susceptibilities.

presence of well-separated excited energy states in **1**. In the case of **2**, the $\chi_M T$ value of $11.33 \text{ cm}^3 \text{ K mol}^{-1}$ at 300 K remains almost constant up to 110 K before gradually decreasing to $10.13 \text{ cm}^3 \text{ K mol}^{-1}$ at 30 K (Fig. 3). Further cooling results in a sharp decrease in $\chi_M T$ value, reaching $8.73 \text{ cm}^3 \text{ K mol}^{-1}$ at 2 K. The field dependence of magnetisation for **2** shows a sharp increase up to 3.0 T, which slowly increases to $4.83 \mu_B$ at 7.0 T without any clear saturation (Fig. S2b and S4†). This observation, in addition to the non-superimposable reduced magnetisation isotherms, indicates the presence of magnetic anisotropy or low-lying excited states in **2**.

Unlike Kramers ions with oblate electron density such as Dy(III), the non-Kramers ions Ho(III) and Tb(III) are prone to exhibit large tunnel splitting leading to faster relaxation. Hence complexes **1** and **2** are perfect examples to verify the

idea, whether the proxy model of the pseudo-linear approach works well with non-Kramers ions or not, in order to obtain high performance SIMs. To probe the slow relaxation dynamics in **1** and **2**, ac susceptibility measurements were carried out along with *ab initio* calculations.

In the case of **1**, both the in-phase (χ'_M) and out-of-phase (χ''_M) components of the ac susceptibilities reveal well-behaved maxima as a function of frequency (ν) and temperature (K) under zero dc field with maxima clearly observable up to 27 K (Fig. 4 and Fig. S5†). The Cole–Cole plots (χ'_M versus χ''_M , Fig. 4c) were fitted using a generalized Debye model for a single relaxation ($0.01 < \alpha < 0.187$). The relaxation times extracted show a temperature dependent regime at higher temperatures ($\ln \tau$ versus T^{-1} , Fig. 4d and Fig. S6†). The relaxation times were modelled with the QTM, direct, Raman and Orbach processes with the following equation:¹⁵

$$\tau^{-1} = \tau_{\text{QTM}}^{-1} + AT + CT^n + \tau_0^{-1} \exp\left(-\frac{U_{\text{eff}}}{k_B T}\right) \quad (1)$$

The best fit to eqn (1) for **1** yields an effective anisotropy barrier, U_{eff} , of 355 K with $\tau_0 = 1.54 \times 10^{-10} \text{ s}$, relative to the Orbach process. It deviates from linearity below 23 K, indicating relaxation assisted *via* an intermediate Raman process ($C = 0.03 \text{ s}^{-1} \text{ K}^{-n}$, $n = 3.5$). The temperature independent regime at lower temperature indicates that quantum tunnelling processes are operative ($\tau_{\text{QTM}} = 1.65 \text{ s}$) (Fig. S6†). This is the largest energy barrier ever reported for a zero-field non-Kramers Ho(III) SMM/SIM (Table 1). However $[\text{Ho}_5\text{O}(\text{O}^i\text{Pr})_{13}]$ displays an energy barrier of 400 K only under an applied high dc field of 3500 Oe.^{5f} Interestingly, the ac susceptibility measurements carried out for **1** under applied dc fields reveal that the relaxation times are independent of the applied field, which is in contrast to the behaviour observed in a large number of reported SIMs/SMMs (Fig. S7–S10†). To further decipher the spin dynamics, we prepared a 10% diluted

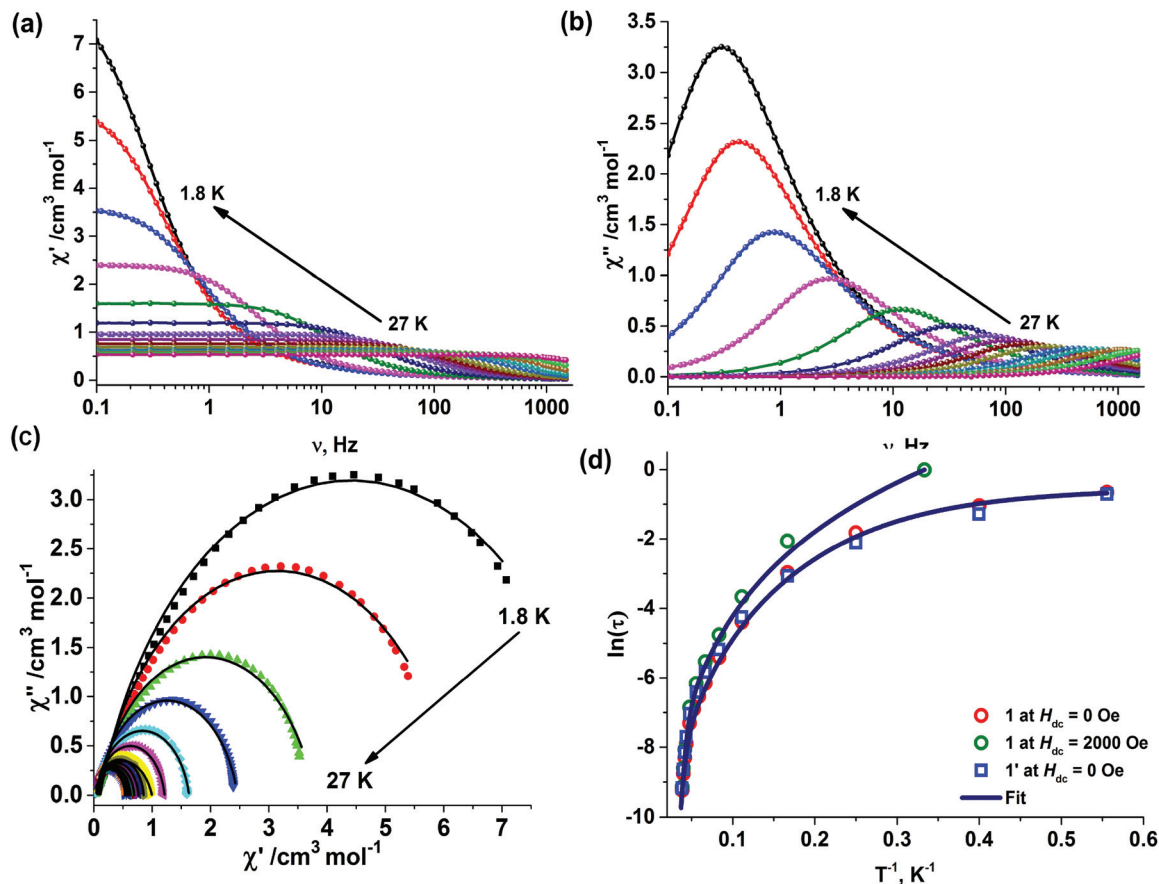


Fig. 4 (a) In-phase (χ') component and (b) out-of-phase (χ'') component of the frequency dependent (0.1–1464 Hz) ac susceptibility measured in the temperature range of 1.8–27 K in an oscillating ac field of 3.5 Oe and zero applied dc field for **1**. (c) Cole–Cole plot for **1** under a zero dc field. (b) Plot of the relaxation time τ (logarithmic scale) versus T^{-1} obtained for **1** at zero applied dc field (red circles), under an applied dc field of 2000 Oe (blue squares) and for **1'** at zero applied dc field (green circles). Solid blue lines represent the best fit to the multiple relaxation processes.

Table 1 Comparison of **1** with monometallic, polymeric and 3d–4f Ho(III) based SMMs

Complex	U_{eff}/K	H_{dc}/Oe	Hysteresis (K)	Field sweep rate/T s ⁻¹	Ref.
1	355	0	4.0	0.027	This work
[Pc ₂ Ho _{0.02} Y _{0.98}][TBA]	—	—	0.5	0.28	5a
[(Cp*)Ho(COT)]	7.4, 3.6	0	—	—	5b
[(Cp*)Ho _{0.05} Y _{0.95} (COT)]	33.8, 24.4	0	—	—	5b
Na ₉ [Ho(W ₅ O ₁₈) ₂ ·xH ₂ O]	—	0	—	—	5c
K ₁₂ [LnP ₅ W ₃₀ O ₁₁₀ ·nH ₂ O]	—	0	2	0.009	5d
[Ho ₄ K ₂ O(O ^t Bu) ₁₂ ·C ₆ H ₁₄]	89.3 ^a , 22.8 ^b	0	—	—	5e
[K(18C6)]{[(Me ₃ Si) ₂ N] ₂ (THF)Ho ₂ (μ-η ² :η ² -N ₂)}	105	0	—	—	2d
[Ho ₅ O(O ⁱ Pr) ₁₃]	400	3500	—	—	5f
HoSc ₂ N@C80	16.5	2000	—	—	5j
[HoL ₂ (H ₂ O) ₅]I ₃ ·2L ¹ ·H ₂ O·EtOH	341	0	3	0.14	5g
[Ho ₄ (μ ₃ -OH) ₂ (L ²) ₄ (piv) ₂ (DMF) ₂ ·2DMF]	21.49	5000	—	—	5h
[L ³ Co ₂ Ho][NO ₃]	8	0	—	—	5i

^a Deduced from relaxation times obtained from frequency dependent ac susceptibility experiment. ^b Deduced from relaxation times obtained from temperature dependent ac susceptibility experiment. 18C6 = 18-crown-6; Pc = dianion of phthalocyanine; TBA = tetra-*n*-butyl ammonium; L₁ = CyPh₂PO; H₂L² = 2-hydroxy-3-methoxyphenylsalicylaldimine; piv = pivalate; Cp* = pentamethylcyclopentadienide; COT = cyclooctatetraene; L³H₃ = (S)P[N(Me)N=CH-C₆H₃-2-OH-3-OMe]₃.

sample (**1'**) in an isomorphous Y(III) analogue.^{3b} **1'** typically reveals similar spin dynamics but the QTM due to intermolecular interactions is basically quenched as seen from

fitting the relaxation times in eqn (1) (Fig. 4d and Fig. S11–S13†). The high anisotropy barrier observed for the Ho(III) SIM prompted us further to measure the field dependent magneti-

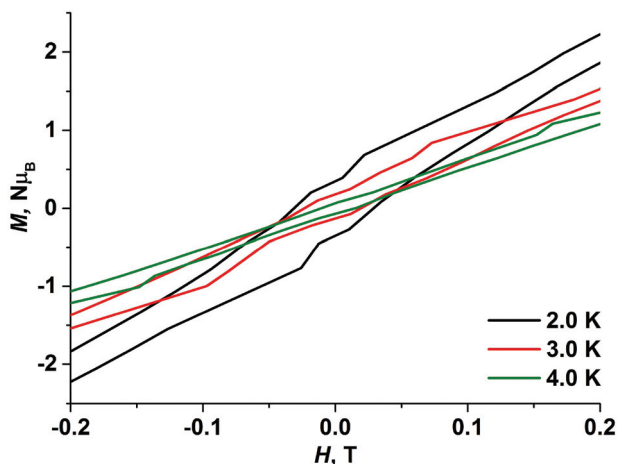


Fig. 5 The field-dependent magnetization data for **1'** at a sweep rate of 0.027 T s^{-1} .

sation. Both **1** and **1'** reveal clear opening up of magnetic hysteresis up to 4.0 K with a coercivity of approximately 500 Oe at 2.0 K (sweep rate, 0.27 T s^{-1}), the highest observed for any Ho(III) or Tb(III) based SIM to date (Fig. 5, Fig. S14† and Table 1).

In contrast, complex **2** with more anisotropic 4f ion (Tb(III)) with a strong axial CF reveals non-zero out-of-phase ac susceptibility (χ''_M) signals below 7 K. Nevertheless, no maxima are observed as a function of frequency (Fig. S15†). This observation is in sharp contrast to the conventional thought that a strong axial CF in a high symmetry would result in high performance SIMs, especially in the case of non-Kramers ions. The application of a dc field of 1500 Oe, however, reveals clear maxima in the out-of-phase (χ''_M) components of the ac susceptibility but the QTM and Raman processes (Fig. 6 and Fig. S17–S19†) dominate the relaxation dynamics.

Electronic structure calculations

To understand the electronic structure of complexes **1** and **2** and to probe the contrasting magnetic properties exhibited by the two non-Kramers ions, we have carried out *ab initio* CASSCF/RASSI-SO/SINGLE_ANISO calculations (see the ESI†

for details) on the X-ray crystal structures. For complex **1**, the pseudo doublets of the ground state possess a g_{zz} value of 19.85, which is close to the expected value of 20. The pure Ising nature of the ground state pseudo doublets (g_{zz}), as well as a negligible tunnel splitting value (0.001 cm^{-1}), signifies the absence of QTM (Table S4†). Furthermore, the wavefunction analysis reveals that the ground state is purely $m_j = \pm 8$, adding support to the absence of QTM (Table S5†). The analysis of CASSCF Mulliken charges shows the accumulation of a large negative charge on the axial oxygen atoms (Table S6†) compared to the equatorial atoms, thus favouring the stabilization of large m_j values as the ground state. The first excited state lies 259.7 cm^{-1} (374.7 K) above the ground state (Table S4†). The tunnel splitting value between these pseudo doublets is large enough (0.85 cm^{-1}) to result in the relaxation *via* the first excited state (Table S4†). The g_{zz} axis of the ground state pseudo doublets is oriented along the Ho–O–P (Fig. 7) whereas the orientation for the first pseudo doublets is close to one of the equatorial oxygens, tilted by an angle of 73.44° , confirming that the relaxation is *via* this excited state (Table S4†). The mixing of $m_j = |\pm 5\rangle$, $m_j = |\pm 4\rangle$, $m_j = |\pm 3\rangle$ and $m_j = |\pm 2\rangle$ states

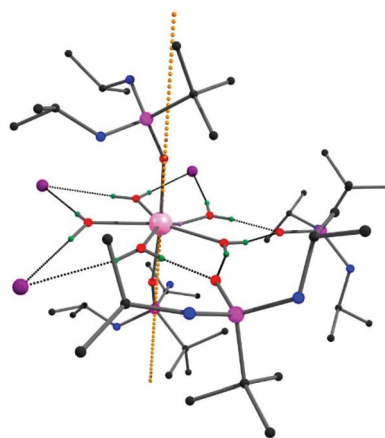


Fig. 7 CASSCF computed g_{zz} orientation of the ground state pseudo doublets in **1** (H atoms in the ligands except the water molecules are omitted for clarity).

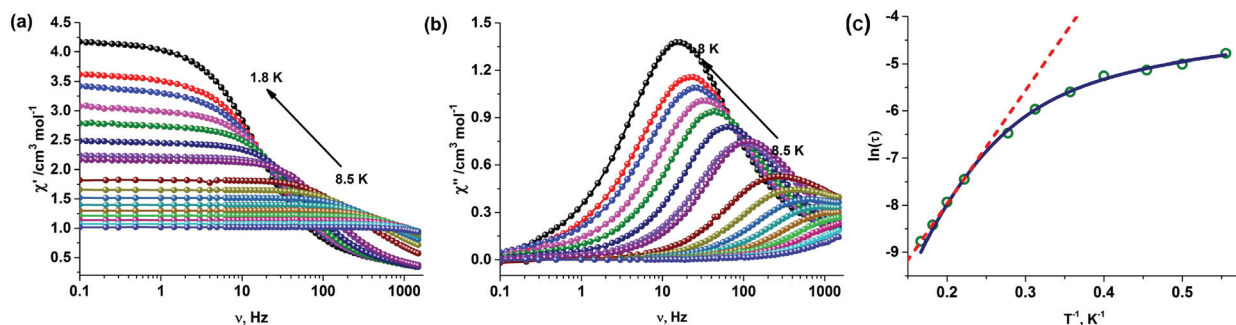


Fig. 6 (a) In-phase (χ'_M) component and (b) out-of-phase (χ''_M) component of the frequency dependent (0.1–1464 Hz) ac susceptibility for **2** measured in an oscillating ac field of 3.5 Oe and under an applied dc field of 1500 Oe. (c) Plot of the relaxation time τ (logarithmic scale) versus T^{-1} obtained; the solid red line corresponds to the best fit to the multiple relaxation equation.

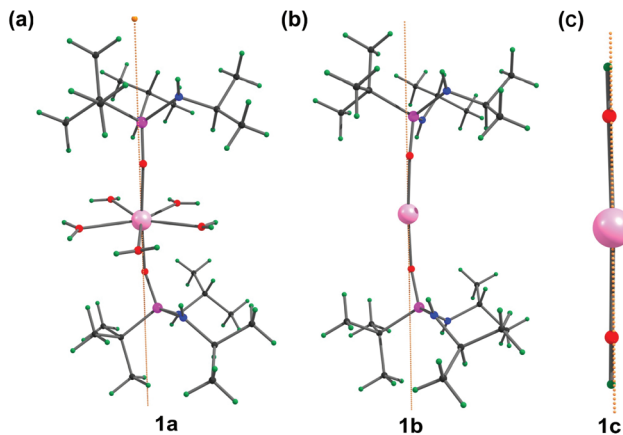


Fig. 8 Modelled structures of **1a** (a), **1b** (b) and **1c** (c).

($|\pm 3\rangle$ and $|\pm 2\rangle$ are the major contributors) in the first excited pseudo states induces the tunnel splitting between the first excited pseudo doublets, resulting in magnetic relaxation (Table S5[†]). The theoretical estimate of the energy barrier (374.7 K) is close to the experimentally observed U_{eff} value, which adds support to the employed methodology.

To find a way to further enhance the energy barrier and to understand the intricate differences in the observed magnetic properties between **1** and **2**, we have performed calculations on three models, **1a** [$\text{L}_2\text{Ho}(\text{H}_2\text{O})_5$], **1b** [L_2Ho] and **1c** [$\text{Ho}(\text{OH})_2$] (see Fig. 8). In model **1a**, only the secondary coordination

sphere entities such as iodine and the free ligands are removed, while in **1b**, the coordinated water molecules are also removed. In model **1c**, the axial ligand is modelled as a hydroxide ion (where a Ho–O distance of 2.19 Å and a nearly linear O–Ho–O angle as in complex **1** are maintained) (Fig. 8c). In all the studied model complexes, (**1a–1c**), $m_j = |\pm 8\rangle$ has been stabilized as the ground state. Although the $m_j = |\pm 8\rangle$ ground state of the Ho(III) ion has strong oblate character, the presence of weak equatorial ligands implies the minimal effect of their electron cloud on 4f ions and their ground state nature. The differences in the energy barriers for model complexes arise mainly from the wavefunction composition of excited m_j levels which is described briefly in the following section. The g tensor of the first excited state in **1a** is 17.28 and the wavefunction analysis shows the stabilization of $m_j = |\pm 7\rangle$ (see Fig. 9 and Tables S7 and S8[†]). For models **1b** and **1c**, as the axial ligands are removed, the wavefunction mixing between different m_j levels at the first excited state disappears leading to quenching of QTM and the sole stabilization of the $m_j = |\pm 7\rangle$ state. At the same time, the ground-state to first excited state energy gap increases significantly in **1b–c** compared to **1** and **1a**. This clearly suggests that the water molecule and the hydrogen bonded iodide ions at the equatorial positions stabilize the lower m_j levels ($m_j = |\pm 3\rangle$ being dominant), as these levels possess electron density along the axial as well as the equatorial directions.^{3a} However, once these equatorial ligands are removed (**1b–c**), $m_j = |\pm 7\rangle$ gets stabilized as the first excited state, pumping the relaxation to higher excited

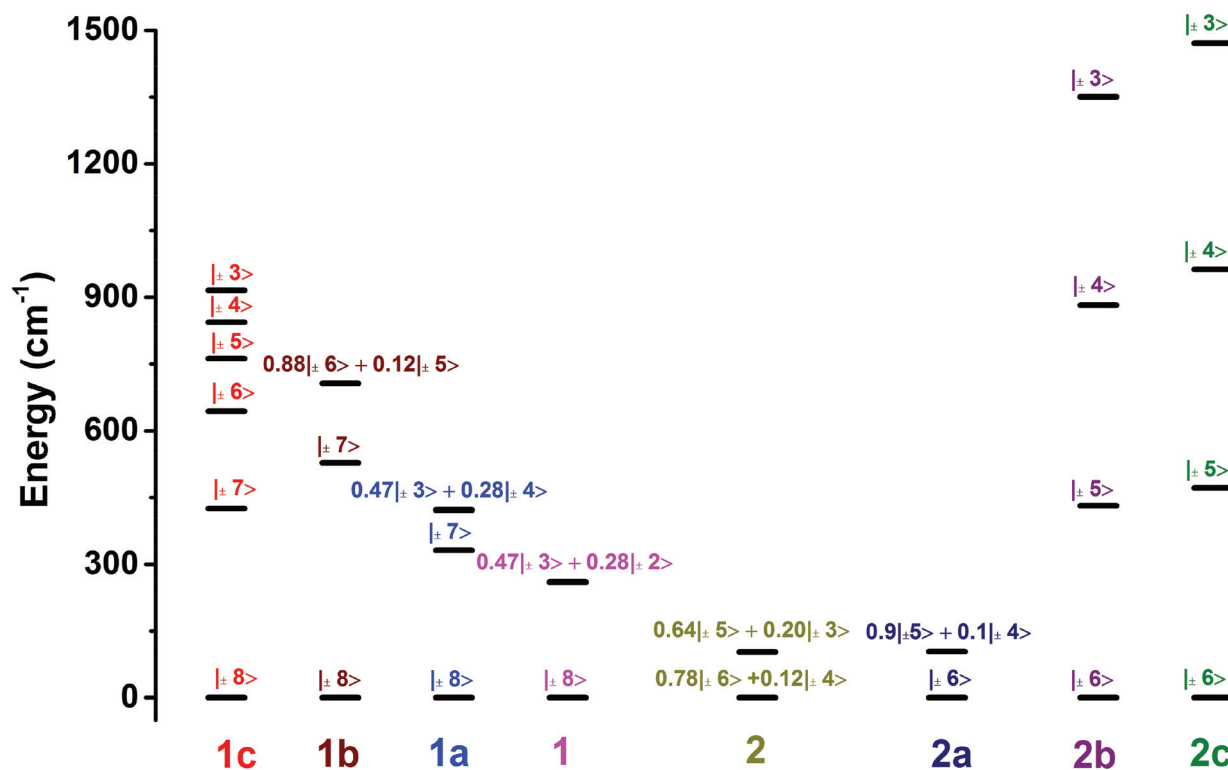


Fig. 9 Energy levels of pseudo doublets for complexes **1a–1c** and **2a–2c** along with their wavefunction compositions.

levels. This clearly demonstrates that the hydrogen bonding along with the second coordination sphere plays a critical role in stabilizing $m_j = |\pm 7\rangle$ in **1a**.

The relative donor strength of the axial oxygen atoms can be estimated from CASSCF computed charges which reveal that oxygen atoms (O1, O2) possess larger negative charges compared to the oxygen atoms of the water molecule (O5–O9). As the iodide ions are removed in **1b**, this significantly reduces the charge on the oxygen of the water molecule leading to a change in the m_j levels (see Table S6 in the ESI†). Even though the tunnelling value for **1a** (0.04) decreases significantly compared to **1** (0.85), the presence of non-negligible tunnelling values leads to relaxation *via* the first excited pseudo doublets (Fig. S20a†) with a considerable increase (478.5 K) in the energy barrier for **1a** compared to **1**. As soon as equatorial water ligands are eliminated (model **1b**) negligible tunneling values for both the ground and the first excited states were obtained, depicting (Table S9†) the possibility of relaxation *via* higher excited states (Fig. S20b†). In model **1c**, we have constructed a highly symmetric $[\text{Ho}(\text{OH})_2]^+$ where $m_j = |\pm 8\rangle$ is found to be the ground state as expected. The higher symmetry and stronger donor interaction pushes the relaxation further to higher excited states as shown in Fig. S20(d).†

The computed energy spectrum and g tensors of complex **2** (Table S13†) reveal that the ground pseudo doublet possesses a g_{zz} value of 16.79 and the wavefunction analysis of this state shows an admixture of $m_j = |\pm 6\rangle$ and $m_j = |\pm 4\rangle$ states (Table S14†). The mixing of the two m_j levels results in a non-negligible tunnel splitting value (0.02 cm^{-1}) and thus induces QTM between the ground pseudo doublet states (Fig. S23a†). This is essentially due to the fact that the $m_j = |\pm 6\rangle$ level is highly anisotropic possessing a disc like density compared to the holmium ion and requires extremely weak or no interaction with the electron cloud from ligands in the equatorial direction to quench QTM efficiently. Although the presence of moderate equatorial and strong axial fields stabilizes the $m_j = |\pm 6\rangle$ level, it mixes strongly with the first excited state. This is in correlation with the observed magnetic properties. This strong mixing induces tunnelling, and quenches the out of phase signals in **2**.

Furthermore, calculations on the corresponding terbium models **2a** $[\text{L}_2\text{Tb}(\text{H}_2\text{O})_5]$, **2b** $[\text{L}_2\text{Tb}]$ ($\text{L} = \text{tBuPO}(\text{NH}^i\text{Pr})_2$) and **2c** $[\text{Tb}(\text{OH})_2]^+$ revealed the role of counter ions in controlling the single-ion magnetic behaviour of **2**. The absence of counter ions and lattice ligands (I^- and phosphoramidate) in **2a** (Table S16†) yields a ground state g_{zz} value of 17.89, which is Ising in nature. Once the equatorial ligands are weakened by removing the iodide ions and the free lattice ligands (as in model **2a**), pure $m_j = |\pm 6\rangle$ is stabilized as the ground state leading to the absence of QTM at this level (Table S16 in ESI†). The reason behind the reduction of mixing and stabilization of the dominant $m_j = |\pm 6\rangle$ level in **2a** (compared to **2**) is also attributed to the decrease in the CASSCF charges of equatorial oxygen atoms (Table S15†). The removal of hydrogen bonding imposed by the second coordination sphere results in the stabilization of a large m_j value as well as a decrease in the tunnelling splitting

value from 0.02 for **2** to 0.001 cm^{-1} for **2a**. This clearly shows that the non-bonding interactions in the second coordination sphere hinder slow relaxation in complex **2**. The first excited state in **2a** is the admixture of $m_j = |\pm 5\rangle$ and $m_j = |\pm 4\rangle$ states (Table S17†). The mixing between the m_j states and the tunnel splitting values implies that the relaxation for this model complex occurs *via* the first excited state (Fig. S23b†). On the other hand, models **2b** and **2c** show lower tunnelling values and a pure m_j state for the first excited state, confirming the relaxation *via* higher excited states (Tables S18, S19, Fig. S23(c, d)†).

At this point, it is worthwhile to compare models **b** and **c** of complexes **1** and **2**. In both these models, equatorial ligands are neglected; therefore these are found to be best suited for strongly anisotropic Tb(III) ions, *i.e.*, models **2b** and **2c** are superior to their counterparts of complex **1** (estimated U_{cal} values for **2b** and **2c** are 1273 and 2122 K, respectively, while that for **1b** and **1c** are 1019 and 1100 K, respectively). However, if weak equatorial ligands are present (such as those in **1**, **2**, **1a** and **2a**), Ho(III) exhibits superior SMM behaviour. As stated above, this is essentially correlated to the individual m_j level electron density, with the Tb(III) $m_j = 6$ exhibiting extreme oblateness and all other m_j levels showing prolate character. Thus it is imperative that the ligand field design (or geometry or symmetry) should be individually catered to different lanthanide ions rather than a blanket definition based only on the largest m_j levels.

Conclusions

The key outcome of this study is the demonstration of an interplay of higher order symmetry and a strong axial CF to design high temperature SIMs even in the case of rare non-Kramers ions such as Ho(III). It has further been shown that this model need not necessarily work for ‘an even more anisotropic non-Kramers ion’ Tb(III). Interestingly, the second coordination sphere, assisted by weak hydrogen bonding, plays a profound role in deciding the SIM behaviour of Ln(III) complexes, resulting in magnetic relaxation *via* the first excited pseudo doublets for **1** and QTM between the ground state pseudo doublets for **2**. *Ab initio* calculations on the model systems reveal that two coordinate Tb(III) would yield larger effective barriers than the Ho(III) analogue. Hence, factors such as crystal field design and controlling the coordination geometry and symmetry apart from the choice of the counter ions will have to be customized for each 4f ion rather than generalized criteria. These combined observations would lead to a better design of novel ligands and their 4f complexes to afford high temperature SIMs, both in the case of Kramers and non-Kramers systems.

Experimental section

Instruments and methods and materials

All the compounds prepared in this study and the starting materials used are air and moisture stable. Hence all the oper-

ations were carried out under aerobic conditions. Solvents were distilled prior to use.¹⁶ Fourier transform infrared spectra were obtained using a PerkinElmer Spectrum One FT-IR spectrometer as KBr diluted discs. Microanalyses were performed on a Thermo Finnigan (FLASH EA 1112) microanalyzer. Thermogravimetric analysis was carried out using a PerkinElmer Pyris Diamond TG/DTA analysis system under a stream of nitrogen gas at a heating rate of 10 °C min⁻¹. The metal content in the samples was measured by inductively coupled plasma atomic emission spectroscopy (ICP-AES). The samples were digested in nitric acid and diluted with distilled water. The magnetic measurements were carried out using a Quantum Design MPMS-XL SQUID magnetometer equipped with a 7 T magnet. Alternating current (ac) susceptibility measurements were carried out at an oscillating ac field of 3.5 Oe and frequencies ranging from 0.1 to 1500 Hz. LnI₃·xH₂O were prepared from Ln₂O₃ (Alfa Aesar). The phosphonic diamide ligand ^tBuPO(NHⁱPr)₂ (L) was synthesized using a previously reported procedure.¹⁴

General procedure for the synthesis of {[L₂Ho(H₂O)₅][I₃·L₂·H₂O]}

To a solution of ^tBuPO(NHⁱPr)₂ (0.330 mg, 1.5 mmol) in a solvent mixture of dichloromethane and benzene (4:1 v/v, 30 mL) was added LnI₃·xH₂O (0.25 mmol). The reaction mixture was stirred at 60 °C for 1 h and was cooled down to room temperature. The solution was allowed to stand for some time and then filtered. The clear filtrate obtained was then kept for crystallization under ambient aerobic conditions. Pale yellow crystals were obtained by the slow evaporation of the solvent mixture within a week. The crystals were carefully washed with toluene.

{[L₂Ho(H₂O)₅][I₃·L₂·H₂O]} (1). Yield: 0.170 g (45%, based on ligand). Anal. calcd for C₄₀H₁₁₂HoI₃N₈O₁₀P₄: C, 31.30; H, 7.36; N, 7.30. Found: C, 31.52; H, 7.46; N, 7.54. FT-IR (KBr, cm⁻¹): 3379 (s), 3290 (br), 2969 (vs), 2872 (m), 1619 (br), 1470 (m), 1420 (s), 1396 (m), 1385 (m), 1368 (m), 1311 (w), 1144 (vs), 1130 (vs), 1114 (vs), 1103 (vs), 1050 (s), 1025 (s), 907 (m), 886 (w), 829 (m), 728 (m), 655 (m), 550 (w), 512 (w).

{[L₂Tb(H₂O)₅][I₃·L₂·H₂O]} (2). Yield: 0.165 g (43%, based on ligand). Anal. calcd for C₄₀H₁₁₂I₃N₈O₁₀P₄Tb₁: C, 31.42; H, 7.38; N, 7.33. Found: C, 31.47; H, 7.24; N, 7.54. FT-IR (KBr, cm⁻¹): 3379 (s), 3290 (br), 2969 (vs), 2872 (m), 1618 (br), 1473 (m), 1470 (m), 1420 (s), 1396 (m), 1386 (m), 1368 (m), 1312 (w), 1144 (vs), 1131 (vs), 1114 (vs), 1100 (vs), 1049 (s), 1025 (s), 906 (m), 886 (w), 829 (m), 720 (m), 655 (m), 550 (w), 512 (w).

Synthesis of {[L₂Ho_{0.10}Y_{0.90}(H₂O)₅][I₃·L₂·H₂O]} (1'). The synthesis of 1' was carried out in a similar way to that described above, the only difference being that a total of 0.25 mmol of triiodide salts of holmium and yttrium was added in a 9:1 ratio. Yield: 0.148 (40%, based on the ligand). Anal. calcd for C₄₀H₁₁₂Ho_{0.1}I₃N₈O₁₀P₄Y_{0.90}: C, 32.76; H, 7.70; N, 7.64. Found: C, 32.82; H, 7.56; N, 7.81. FT-IR (KBr, cm⁻¹): 3384 (s), 3292 (br), 2968 (s), 2871 (m), 1618 (br), 1476 (m), 1470 (m), 1420 (s), 1398 (m), 1386 (m), 1368 (m), 1312 (w), 1144 (vs), 1131 (vs),

1114 (vs), 1101 (vs), 1049 (s), 1025 (s), 907 (w), 887 (w), 830 (w), 727 (w), 678 (w), 655 (w), 544 (w), 513 (w).

Single crystal X-ray crystallography

Suitable single crystals of the compounds were selected and mounted on a Rigaku Saturn 724+ CCD diffractometer using Paratone oil for unit cell determination and three dimensional intensity data collection. Data integration and indexing was carried out using CrystalClear and CrystalStructure.¹⁷ The structures were solved by direct methods (SIR-97).¹⁸ Structure refinement and geometrical calculations were carried out using the programs in the WinGX module and Olex2 v1.2.¹⁹ The final structure refinement was carried out using full least-squares methods on *F*² using SHELXL-2014.²⁰ Details of the crystal data and structure refinement of the isomorphous compounds are given in Table 2.

Magnetic studies

The magnetic properties of 1, 2 and 1' were measured using a Quantum Design MPMS-XL SQUID magnetometer equipped with a 7 T magnet in the temperature range 2–300 K using polycrystalline powder samples. The data were corrected for the background diamagnetic contribution and the diamagnetic contribution of the compounds was corrected using Pascal's constants. Alternating current (ac) susceptibility measurements were performed with an oscillating a.c. field of 3.5 Oe oscillating at the indicated frequencies between 0.1 and 1464 Hz.

Computational details

Ab initio calculations have been carried out on complexes 1 and 2 to compute the *g*-tensors and the energies of the non-Kramers pseudo doublets. All the calculations have been performed using the MOLCAS 8.0²¹ quantum chemistry package. In this multi-configurational approach, a relativistic approach has been treated based on the Douglas–Kroll Hamiltonian. We have employed an atomic natural (ANO-RCC) basis set for the calculation of the *g*-tensor. The following contraction schemes have been employed: [8s7p5d3f2g1h] for Ho and Tb, [3s2p] for N, [4s3p2d1f] for O, [4s3p] for P, [3s2p] for C and [2s] for H. The ground state atomic multiplicity of Ho^{III} is ⁵I₈. The CASSCF calculation comprises an active space of ten active electrons in the seven active orbitals (CAS (10,7)). The CASSCF calculations have been performed with 35 quintets, 210 triplets and 196 singlets. In the next step we mixed these CASSCF computed spin-free states *via* the RASSI-SO module to obtain the spin-orbit states. Here we have performed RASSI-SO calculations with 35 quintets, 117 triplets and 75 singlet states and extracted the relative energies of pseudo doublets. On the other hand, the ground state f-electron configuration for Tb^{III} is 4f⁸ and this yields ⁷F₆ as the ground state. First, we performed CASSCF calculations with an active space of eight active electrons in seven 4f orbitals (8,7). With this active space, we computed 7 septets, 140 quintets and 195 triplet states in the CI (Configuration Interaction) procedure. After computing these excited states, we have mixed all these 7

Table 2 Crystallographic refinement data for 1, 2 and 1'

Compound	1	2	1'
Identification code	SKG941	SKG946	SKG-Ho-Y
Empirical formula	C ₄₀ H ₁₁₂ HoI ₃ N ₈ O ₁₀ P ₄	C ₄₀ H ₁₁₂ I ₃ N ₈ O ₁₀ P ₄ Tb	C ₄₀ H ₁₁₂ Ho _{0.1} I ₃ N ₈ O ₁₀ P ₄ Y _{0.9}
Formula weight	1534.88	1528.87	1466.67
Crystal system	Triclinic	Triclinic	Triclinic
Space group	<i>P</i> $\bar{1}$	<i>P</i> $\bar{1}$	<i>P</i> $\bar{1}$
<i>a</i> (Å)	13.7114(1)	13.789(2)	13.743(2)
<i>b</i> (Å)	14.6838(1)	14.794(2)	14.745(2)
<i>c</i> (Å)	20.570(3)	20.679(4)	20.690(4)
<i>a</i> (°)	92.207(1)	92.515(2)	92.443(1)
<i>b</i> (°)	108.127(1)	108.184(1)	108.156(1)
<i>g</i> (°)	115.1480(1)	115.182(1)	114.930(1)
Volume (Å ³)	3492.0(7)	3549.4(1)	3538.3(1)
<i>Z</i>	2	2	2
Crystal size (mm ³)	0.26 × 0.18 × 0.14	0.17 × 0.12 × 0.06	0.24 × 0.18 × 0.07
Reflections collected	37 508	37 426	26 870
Independent reflections	19 931 [<i>R</i> (int) = 0.0295]	19 979 [<i>R</i> (int) = 0.0372]	12 193 [<i>R</i> (int) = 0.0493]
Data/restraints/parameters	19 931/0/703	19 979/5/698	12 193/0/631
Goodness-of-fit on <i>F</i> ²	1.073	1.054	1.092
Final <i>R</i> indices [<i>I</i> > 2σ(<i>I</i>)]	<i>R</i> ₁ = 0.0443, <i>wR</i> ₂ = 0.0844	<i>R</i> ₁ = 0.0462, <i>wR</i> ₂ = 0.1012	<i>R</i> ₁ = 0.0802, <i>wR</i> ₂ = 0.2534
<i>R</i> indices (all data)	<i>R</i> ₁ = 0.0517, <i>wR</i> ₂ = 0.0906	<i>R</i> ₁ = 0.0497, <i>wR</i> ₂ = 0.1047	<i>R</i> ₁ = 0.0906, <i>wR</i> ₂ = 0.2582
Largest diff. peak and hole (e Å ⁻³)	1.317 and -2.331	1.507 and -2.671	3.229 and -1.742

septets, 105 quintets and 112 triplets using the RASSI-SO module to compute the spin-orbit coupled states. In the last step we used the SINGLE_ANISO code²² implemented in the MOLCAS to compute the *g*-tensors of Ho^{III} and Tb^{III} ions. Furthermore, our computed molar magnetic susceptibility and molar magnetization have been computed and are found to be nicely agreeing with experimental observations.

Conflicts of interest

There are no conflicts to declare.

Acknowledgements

This work was supported by the SERB, New Delhi (SB/S2/JCB-85/2014, SB/S1/IC-48/2013 and SR/NM/NS-1119/2011). GR would like to thank the INSA, SERB (EMR/2014/000247) for financial support. The authors acknowledge Prof. Lorenzo Sorace, Florence, for fruitful discussions. We acknowledge Dr L. Ungur and Prof. L. F. Chibotaru, Belgium for additional MOLCAS routines. S. K. G. thanks the UGC and DST, New Delhi for a research fellowship.

Notes and references

- (a) M. Mannini, F. Pineider, P. Sainctavit, C. Danieli, E. Otero, C. Sciancalepore, A. M. Talarico, M.-A. Arrio, A. Cornia, D. Gatteschi and R. Sessoli, *Nat. Mater.*, 2009, **8**, 194–197; (b) M. Urdampilleta, S. Klyatskaya, J. P. Cleuziou, M. Ruben and W. Wernsdorfer, *Nat. Mater.*, 2011, **10**, 502–506; (c) R. Vincent, S. Klyatskaya, M. Ruben, W. Wernsdorfer and F. Balestro, *Nature*, 2012, **488**, 357–360.
- (a) J. D. Rinehart, M. Fang, W. J. Evans and J. R. Long, *Nat. Chem.*, 2011, **3**, 538–542; (b) S. K. Langley, D. P. Wielechowski, B. Moubaraki and K. S. Murray, *Chem. Commun.*, 2016, **52**, 10976–10979; (c) S. K. Langley, D. P. Wielechowski, V. Vieru, N. F. Chilton, B. Moubaraki, L. F. Chibotaru and K. S. Murray, *Chem. Sci.*, 2014, **5**, 3246–3256; (d) J. D. Rinehart, M. Fang, W. J. Evans and J. R. Long, *J. Am. Chem. Soc.*, 2011, **133**, 14236–14239.
- (a) J. D. Rinehart and J. R. Long, *Chem. Sci.*, 2011, **2**, 2078–2085; (b) S. K. Gupta, T. Rajeshkumar, G. Rajaraman and R. Murugavel, *Chem. Sci.*, 2016, **7**, 5181–5191; (c) W.-B. Sun, P.-F. Yan, S.-D. Jiang, B.-W. Wang, Y.-Q. Zhang, H.-F. Li, P. Chen, Z.-M. Wang and S. Gao, *Chem. Sci.*, 2016, **7**, 684–691; (d) Y.-S. Ding, N. F. Chilton, R. E. P. Winpenny and Y.-Z. Zheng, *Angew. Chem., Int. Ed.*, 2016, **55**, 16071–16074; (e) J. Liu, Y.-C. Chen, J.-L. Liu, V. Vieru, L. Ungur, J.-H. Jia, L. F. Chibotaru, Y. Lan, W. Wernsdorfer, S. Gao, X.-M. Chen and M.-L. Tong, *J. Am. Chem. Soc.*, 2016, **138**, 5441–5450; (f) M. Gregson, N. F. Chilton, A.-M. Ariciu, F. Tuna, I. F. Crowe, W. Lewis, A. J. Blake, D. Collison, E. J. L. McInnes, R. E. P. Winpenny and S. T. Liddle, *Chem. Sci.*, 2016, **7**, 155–165; (g) Y.-C. Chen, J.-L. Liu, L. Ungur, J. Liu, Q.-W. Li, L.-F. Wang, Z.-P. Ni, L. F. Chibotaru, X.-M. Chen and M.-L. Tong, *J. Am. Chem. Soc.*, 2016, **138**, 2829–2837; (h) S. K. Gupta, T. Rajeshkumar, G. Rajaraman and R. Murugavel, *Chem. Commun.*, 2016, **52**, 7168–7171; (i) J.-L. Liu, Y.-C. Chen, Y.-Z. Zheng, W.-Q. Lin, L. Ungur, W. Wernsdorfer, L. F. Chibotaru and M.-L. Tong, *Chem. Sci.*, 2013, **4**, 3310–3316; (j) F.-S. Guo, B. M. Day, Y.-C. Chen, M.-L. Tong, A. Mansikkamäki and R. A. Layfield, *Angew. Chem., Int. Ed.*, 2017, **56**, 11445–11449.
- (a) F. Pointillart, O. Cadour, B. Le Guennic and L. Ouahab, *Coord. Chem. Rev.*, 2017, **346**, 150–175; (b) D. N. Woodruff,

- R. E. P. Winpenny and R. A. Layfield, *Chem. Rev.*, 2013, **113**, 5110–5148; (c) T. Pugh, N. F. Chilton and R. A. Layfield, *Angew. Chem., Int. Ed.*, 2016, **55**, 11082–11085; (d) L. Ungur, J. J. Le Roy, I. Korobkov, M. Murugesu and L. F. Chibotaru, *Angew. Chem., Int. Ed.*, 2014, **53**, 4413–4417; (e) S. G. McAdams, A.-M. Ariciu, A. K. Kostopoulos, J. P. S. Walsh and F. Tuna, *Coord. Chem. Rev.*, 2017, **346**, 216–239.
- 5 (a) N. Ishikawa, M. Sugita and W. Wernsdorfer, *J. Am. Chem. Soc.*, 2005, **127**, 3650–3651; (b) S.-D. Jiang, S.-S. Liu, L.-N. Zhou, B.-W. Wang, Z.-M. Wang and S. Gao, *Inorg. Chem.*, 2012, **51**, 3079–3087; (c) M. A. AlDamen, S. Cardona-Serra, J. M. Clemente-Juan, E. Coronado, A. Gaita-Ariño, C. Martí-Gastaldo, F. Luis and O. Montero, *Inorg. Chem.*, 2009, **48**, 3467–3479; (d) S. Cardona-Serra, J. M. Clemente-Juan, E. Coronado, A. Gaita-Ariño, A. Camón, M. Evangelisti, F. Luis, M. J. Martínez-Pérez and J. Sesé, *J. Am. Chem. Soc.*, 2012, **134**, 14982–14990; (e) R. J. Blagg, L. Ungur, F. Tuna, J. Speak, P. Comar, D. Collison, W. Wernsdorfer, E. J. L. McInnes, L. F. Chibotaru and R. E. P. Winpenny, *Nat. Chem.*, 2013, **5**, 673–678; (f) R. J. Blagg, F. Tuna, E. J. L. McInnes and R. E. P. Winpenny, *Chem. Commun.*, 2011, **47**, 10587–10589; (g) Y.-C. Chen, J.-L. Liu, W. Wernsdorfer, D. Liu, L. F. Chibotaru, X.-M. Chen and M.-L. Tong, *Angew. Chem., Int. Ed.*, 2017, **56**, 4996–5000; (h) W.-W. Kuang, L.-L. Zhu, Y. Xu and P.-P. Yang, *Inorg. Chem. Commun.*, 2015, **61**, 169–172; (i) V. Chandrasekhar, B. M. Pandian, J. J. Vittal and R. Clérac, *Inorg. Chem.*, 2009, **48**, 1148–1157; (j) J. Dreiser, R. Westerström, Y. Zhang, A. A. Popov, L. Dunsch, K. Krämer, S.-X. Liu, S. Decurtins and T. Greber, *Chem. – Eur. J.*, 2014, **20**, 13536–13540.
- 6 (a) N. F. Chilton, C. A. P. Goodwin, D. P. Mills and R. E. P. Winpenny, *Chem. Commun.*, 2015, **51**, 101–103; (b) N. F. Chilton, *Inorg. Chem.*, 2015, **54**, 2097–2099; (c) S. K. Singh, T. Gupta and G. Rajaraman, *Inorg. Chem.*, 2014, **53**, 10835–10845; (d) T. Gupta and G. Rajaraman, *J. Chem. Sci.*, 2014, **126**, 1569–1579.
- 7 (a) C. A. P. Goodwin, F. Ortu, D. Reta, N. F. Chilton and D. P. Mills, *Nature*, 2017, **548**, 439–442; (b) R. Sessoli, *Nature*, 2017, **548**, 400–401.
- 8 A. Upadhyay, S. K. Singh, C. Das, R. Mondol, S. K. Langley, K. S. Murray, G. Rajaraman and M. Shanmugam, *Chem. Commun.*, 2014, **50**, 8838–8841.
- 9 (a) N. Ishikawa, M. Sugita, T. Ishikawa, S.-Y. Koshihara and Y. Kaizu, *J. Am. Chem. Soc.*, 2003, **125**, 8694–8695; (b) S. Takamatsu, T. Ishikawa, S.-Y. Koshihara and N. Ishikawa, *Inorg. Chem.*, 2007, **46**, 7250–7252.
- 10 (a) S.-D. Jiang, B.-W. Wang, H.-L. Sun, Z.-M. Wang and S. Gao, *J. Am. Chem. Soc.*, 2011, **133**, 4730–4733; (b) K. R. Meihaus and J. R. Long, *J. Am. Chem. Soc.*, 2013, **135**, 17952–17957; (c) J. J. Le Roy, L. Ungur, I. Korobkov, L. F. Chibotaru and M. Murugesu, *J. Am. Chem. Soc.*, 2014, **136**, 8003–8010.
- 11 C. R. Ganivet, B. Ballesteros, G. de la Torre, J. M. Clemente-Juan, E. Coronado and T. Torres, *Chem. – Eur. J.*, 2013, **19**, 1457–1465.
- 12 T. Gupta, G. Velmurugan, T. Rajeshkumar and G. Rajaramna, *J. Chem. Sci.*, 2016, **128**, 1615–1630.
- 13 M. Shiddiq, D. Komijani, Y. Duan, A. Gaita-Ariño, E. Coronado and S. Hill, *Nature*, 2016, **531**, 348–351.
- 14 R. Murugavel and R. Pothiraja, *New J. Chem.*, 2003, **27**, 968–974.
- 15 (a) E. Lucaccini, L. Sorace, M. Perfetti, J.-P. Costes and R. Sessoli, *Chem. Commun.*, 2014, **50**, 1648–1651; (b) A. J. Brown, D. Pinkowicz, M. R. Saber and K. R. Dunbar, *Angew. Chem., Int. Ed.*, 2015, **54**, 5864–5868; (c) K. S. Pedersen, L. Ungur, M. Sigrist, A. Sundt, M. Schau-Magnussen, V. Vieru, H. Mutka, S. Rols, H. Weihe, O. Waldmann, L. F. Chibotaru, J. Bendix and J. Dreiser, *Chem. Sci.*, 2014, **5**, 1650–1660.
- 16 W. L. F. Armarego, *Purification of laboratory chemicals/W.L.F. Armarego and D.D. Perrin*, Butterworth Heinemann, Oxford, Boston, 1996.
- 17 *CrystalClear, Version-SM Expert 2.0 r4, 2009 and CrystalStructure, Version 4.0*, Rigaku, Rigaku Americas and Rigaku, The Woodlands, 2010, Texas, USA and Rigaku Corporation, Tokyo, Japan.
- 18 A. Altomare, M. C. Burla, M. Camalli, G. L. Casciarano, C. Giacovazzo, A. Guagliardi, A. G. G. Moliterni, G. Polidori and R. Spagna, *J. Appl. Crystallogr.*, 1999, **32**, 115–119.
- 19 (a) L. Farrugia, *J. Appl. Crystallogr.*, 2012, **45**, 849–854; (b) O. V. Dolomanov, L. J. Bourhis, R. J. Gildea, J. A. K. Howard and H. Puschmann, *J. Appl. Crystallogr.*, 2009, **42**, 339–341.
- 20 G. Sheldrick, *Acta Crystallogr., Sect. C: Struct. Chem.*, 2015, **71**, 3–8.
- 21 (a) F. Aquilante, L. De Vico, N. Ferre, G. Ghigo, P. A. Malmqvist, P. Neogrady, T. B. Pedersen, M. Pitonak, M. Reiher, B. O. Roos, L. Serrano-Andres, M. Urban, V. Veryazov and R. Lindh, *J. Comput. Chem.*, 2010, **31**, 224–247; (b) V. Veryazov, P.-O. Widmark, L. Serrano-Andrés, R. Lindh and B. O. Roos, *Int. J. Quantum Chem.*, 2004, **100**, 626–635; (c) J. A. Duncan, *J. Am. Chem. Soc.*, 2009, **131**, 2416–2416; (d) G. Karlström, R. Lindh, P.-Å. Malmqvist, B. O. Roos, U. Ryde, V. Veryazov, P.-O. Widmark, M. Cossi, B. Schimmelpfennig, P. Neogrady and L. Seijo, *Comput. Mater. Sci.*, 2003, **28**, 222–239.
- 22 L. Chibotaru and L. Ungur, *The computer programs SINGLE_ANISO and POLY_ANISO*, University of Leuven, 2.